

Article

## Automatic Geographic Object Based Mapping of Streambed and Riparian Zone Extent from LiDAR Data in a Temperate Rural Urban Environment, Australia

Kasper Johansen <sup>1,\*</sup>, Dirk Tiede <sup>2</sup>, Thomas Blaschke <sup>2</sup>, Lara A. Arroyo <sup>3</sup> and Stuart Phinn <sup>1</sup>

<sup>1</sup> Joint Remote Sensing Research Program, Centre for Spatial Environmental Research, School of Geography and Environmental Management, The University of Queensland, Brisbane, QLD 4072, Australia; E-Mail: s.phinn@uq.edu.au

<sup>2</sup> Z\_GIS Centre for Geoinformatics, Salzburg University, Schillerstrasse 30, 5020 Salzburg, Austria; E-Mails: dirk.tiede@sbg.ac.at (D.T.); thomas.blaschke@sbg.ac.at (T.B.)

<sup>3</sup> Centro de Investigacion del Fuego, Fundacion General del Medio Ambiente de Castilla La Mancha, 45071 Toledo, Spain; E-Mail: lara.arroyo@uclm.es

\* Author to whom correspondence should be addressed; E-Mail: k.johansen@uq.edu.au; Tel.: +61-7-3346-7016; Fax: +61-7-3365-6899.

Received: 12 April 2011; in revised form: 5 May 2011 / Accepted: 17 May 2011 /

Published: 30 May 2011

---

**Abstract:** This research presents a time-effective approach for mapping streambed and riparian zone extent from high spatial resolution LiDAR derived products, *i.e.*, digital terrain model, terrain slope and plant projective cover. Geographic object based image analysis (GEOBIA) has proven useful for feature extraction from high spatial resolution image data because of the capacity to reduce effects of reflectance variations of pixels making up individual objects and to include contextual and shape information. This functionality increases the likelihood of developing transferable and automated mapping approaches. LiDAR data covered parts of the Werribee Catchment in Victoria, Australia, which is characterized by urban, agricultural, and forested land cover types. Field data of streamside vegetation structure and physical form properties were used for both calibration of the mapping routines and validation of the mapping results. To improve the transferability of the rule set, the GEOBIA approach was developed for an area representing different riparian zone environments, *i.e.*, urbanized, agricultural and hilly forested areas. Results show that mapping streambed extent ( $R^2 = 0.93$ , RMSE = 3.6 m,  $n = 35$ ) and riparian zone extent ( $R^2 = 0.74$ , RMSE = 3.9,  $n = 35$ ) from LiDAR derived

products can be automated using GEOBIA to enable derivation of spatial information in an accurate and time-effective manner suited for natural resource management agencies.

**Keywords:** geographic object based image analysis (GEOBIA); LiDAR; streambed; riparian zone; Australia; pixel-based object resizing

---

## 1. Introduction

### 1.1. Riparian Zones

Riparian zones along rivers and creeks have long been identified as important elements of the landscape due to the flow of species, energy, and nutrients, and their provision of corridors providing an interface between terrestrial and aquatic ecosystems [1,2]. Threats to riparian zones are compounded by increased anthropogenic development and disturbances in or adjacent to these environments. Riparian zones and related vegetation form corridors with distinct environmental functions and processes. To assess these functions and processes environmental indicators of riparian vegetation structure and physical form of stream banks are normally used [3]. Two of the most important environmental indicators to assess are streambed extent and riparian zone extent, as these allow further assessment of riparian environmental indicators within the stream and riparian zones [4]. Mapping streambed extent allows determination and assessment of a number of riparian environmental indicators such as streambed width, vegetation overhanging the stream, identification of stream banks for stream bank condition assessment, and water body assessment. Mapping the extent of the riparian zones defines the area within which riparian environmental indicators such as riparian zone width, plant projective cover, *i.e.*, the percentage of ground area covered by the vertical projection of leaves and branches (PPC), vegetation continuity, and other vegetation structural parameters are to be assessed. Hence, a starting point and requirement for riparian zone assessment is the accurate mapping and identification of streambed and riparian zone extents.

### 1.2. Remote Sensing of Riparian Zones

Several papers have concluded that the use of remotely sensed image data is required for the assessment of riparian zones for areas >200 km of stream length, as field surveys become cost prohibitive at those spatial scales [5]. The availability of data from high spatial resolution sensors such as the IKONOS, QuickBird and GeoEye-1 satellite sensors and airborne multi-spectral, hyper-spectral and light detection and ranging (LiDAR) sensors have opened up new opportunities for development of operational mapping and monitoring of small features such as narrow riparian zones [6,7]. Johansen *et al.* [8,9] found airborne LiDAR data to be suitable for mapping a number of riparian environmental indicators. They also assessed the use of LiDAR data for mapping streambed and riparian zone extents using geographic object based image analysis (GEOBIA) and obtained high mapping accuracies of streambed and riparian zone widths [8]. However, the rule sets applied to automatically map streambed and riparian zone extents were found time-consuming, especially for large area mapping because of the use of near pixel-level segmentations and region growing

algorithms. The rule sets were also found to work only in areas with streambeds clearly defined by bordering steep bank slopes.

### 1.3. Geographic Object Based Image Analysis

Object based approaches are increasingly used in image processing and particularly in the geospatial domain. Blaschke and Strobl [10] identified an increasing dissatisfaction with per-pixel image analysis. Although this critique was not new [10-12], Blaschke [13] analyzed whether this trend is significant within remote sensing and found that there is a hype in applications built on image segmentation, *i.e.*, the partitioning of an image into meaningful geographically based objects [10,14-17]. Image segmentation is not a new approach [18,19], but it was not used extensively in geospatial applications throughout the 1980s and 1990s [12]. Today, GEOBIA is somehow matured and it is widely agreed [10-12,14-16,20-22] that object based image analysis builds on segmentation, edge-detection, feature extraction and classification concepts that have been used in remote sensing image analysis for decades [18,23].

Within remote sensing applications, segmentation algorithms are numerous and have been rapidly increasing over the past few years [12,24]. Image segmentation, from an algorithmic perspective, is generally divided into four categories: (a) point-based; (b) edge-based; (c) region-based; and (d) combined [19]. Segmentation provides the building blocks of GEOBIA [16,22]. Segments are regions which are generated by one or more criteria of homogeneity in one or more dimensions of a feature space respectively. Thus segments have additional spectral information compared to single pixels (e.g., mean values per band, median values, minimum and maximum values, mean ratios, variance, *etc.*), but of even greater advantage than the diversification of spectral value descriptions of objects is the additional spatial information of objects [10,14,22,25]. This spatial dimension (distances, neighborhood, shape, topologies, *etc.*) is crucial to GEOBIA methods, and this is a major reason for the marked increase in the use of segmentation based methods in recent times, compared to the use of image segmentation in remote sensing during the 1980s and 1990s [12,14,15,20]. It is this additional information and the reduction of feature reflectance variation at the object level that make object based feature extraction and conversion of image data sets into thematic map products so unique.

GEOBIA is associated with 'high spatial resolution situations', where the pixels are significantly smaller than the objects under consideration [13]. Only then, regionalization of pixels into groups of pixels and finally objects is useful and needed. GEOBIA also provides a bridge between the spatial concepts applied in multi-scale landscape analysis [11,26], Geographic Information Systems (GIS) and the synergy between image objects and their radiometric characteristics and analyses in Earth Observation data. In fact, for the past 10 years, a major emphasis has been placed on GEOBIA approaches for mapping and monitoring earth surface objects and phenomena to achieve greater efficiency and objectivity, which are inherent to such approaches [12,27-32].

This paper builds on the GEOBIA concept when making up individual objects while including contextual and shape information. In the next sub-sections, it is demonstrated that objects and object based analyses allow for the characterization of topography and ecosystem structure from LiDAR derived products. The objective of this work was to develop a new, time-effective and transferable approach for mapping streambed and riparian zone extents from high spatial resolution LiDAR derived

products, *i.e.*, digital terrain model (DTM), terrain slope and PPC for a complex rural urban area in Victoria, Australia using GEOBIA. Within the study area the riparian zones were located in urbanized, agricultural and forested areas with varying levels of topographic terrain slope and aspect.

## 2. Data and Methods

### 2.1. Study Area

The riparian study area was located along the Werribee and Lerderderg Rivers and Pyrites, Djerriwarrh, and Parwan Creeks in the urbanized and cultivated temperate Werribee Catchment in Victoria, 50 km northwest of Melbourne. The extent of the study area covered approximately 59 km of stream length (Figure 1). The Werribee River is the major drainage stream emanating from the Werribee Catchment, and the rivers and creeks nominated for the study area confluence with it. In the northern part of the study area remnant forests of the Central Victorian Upland bioregion exist. The northern terrain is characterized by small streams cutting courses and gorges in heavily eroded hills. The water flow of the streams is generally south from the hilly areas until reaching the confluence with the Werribee River, where flows turns east and then southeast before eventually draining into Port Phillip Bay. The southern half of the study area is part of the flat Victorian Volcanic Plain bioregion characterized by disturbed terrain with agricultural (grazing and cultivation) and urban land use features.

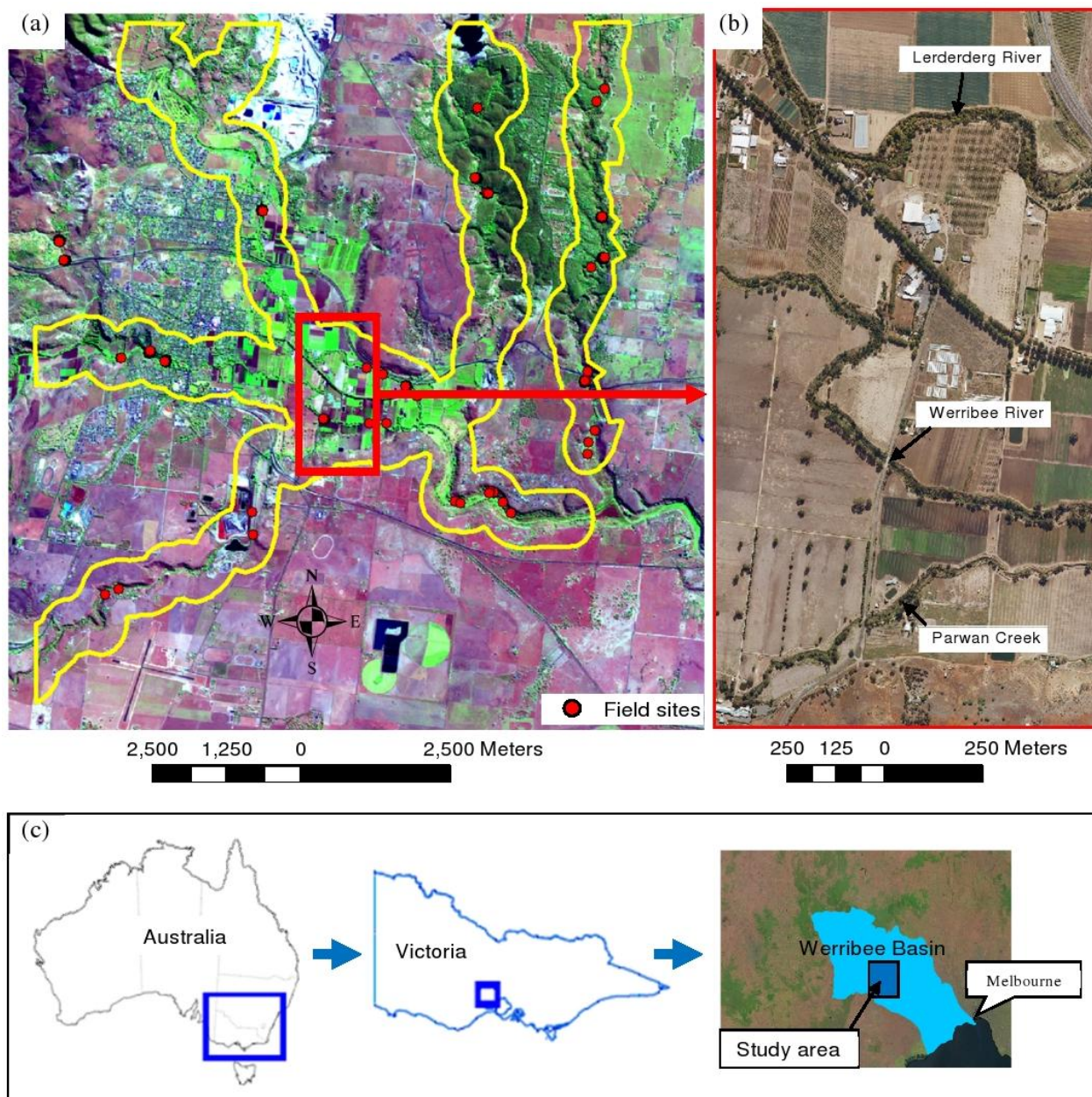
The study area includes two main geomorphic river types representing (1) partly confined valleys with discontinuous floodplain with the channel impinging on the valley margin and (2) alluvial channels of low sinuosity with fine grained bed and bank sediments with the channel rarely impinging on the valley margins. The northern most parts of the study area belong to the partly confined valleys with streambed material varying between bedrock and sand. The sections of the streams in the downstream parts of the study area with less topographic variation consist of alluvial material of gravel and coarse sediments. These sections of the streams are generally stable when vegetated but are highly unstable if modified and susceptible to avulsion at high flow stages [33].

### 2.2. Field Data Acquisition

A field campaign was carried out in the Werribee Catchment between 31 March and 4 April 2008. The field data acquisition was designed to match the spatial resolution of the LiDAR data. Field measurements were obtained of several biophysical vegetation structural and physical form parameters along one transect for each of the 35 field sites (Figure 1). The transects were located perpendicular to the streams and ranged in length from 15 m to 85 m to cover the full width of the riparian zones. However, the only field measurements used in this research included: (1) streambed width; (2) riparian zone width; (3) PPC; and (4) stream bank slope and elevation. Streambed width was measured with a laser range finder. Riparian zone width was measured with a tape measure from the toe of the stream bank to the external perimeter defined by the stream bank flattening and the vegetation species that no longer dependent on the stream for survival. GPS point measurements were obtained by averaging the position of the start and end of each transect until the estimated positional error was below 2.0 m. Existing airborne high spatial resolution optical image data geometrically referenced to the LiDAR

data (RMSE = 0.85 m) were used to complement GPS points by identifying features visible in both the field and image data to precisely overlay the two data sets.

**Figure 1.** (a) Area covered by the LiDAR data (outlined in yellow) in the Werribee Catchment; (b) zoomed in section of UltracamD image data showing more details of the Lerderderg River (north), Werribee River (middle), and Parwin Creek (south) and (c) study area location within the Werribee Basin, Victoria, Australia. Thirty-five field plots were assessed. A SPOT-5 image is used as a backdrop to illustrate the LiDAR data coverage.



### 2.3. LiDAR Data Acquisition and Preparation

The LiDAR data used in this study were captured using the Optech ALTM3025 sensor between 7 and 9 May 2005 for the study area. The LiDAR data were captured with an average point spacing of 1.6 m (0.625 points per m<sup>2</sup>) and consisted of the first and last returns and raw intensity. The LiDAR

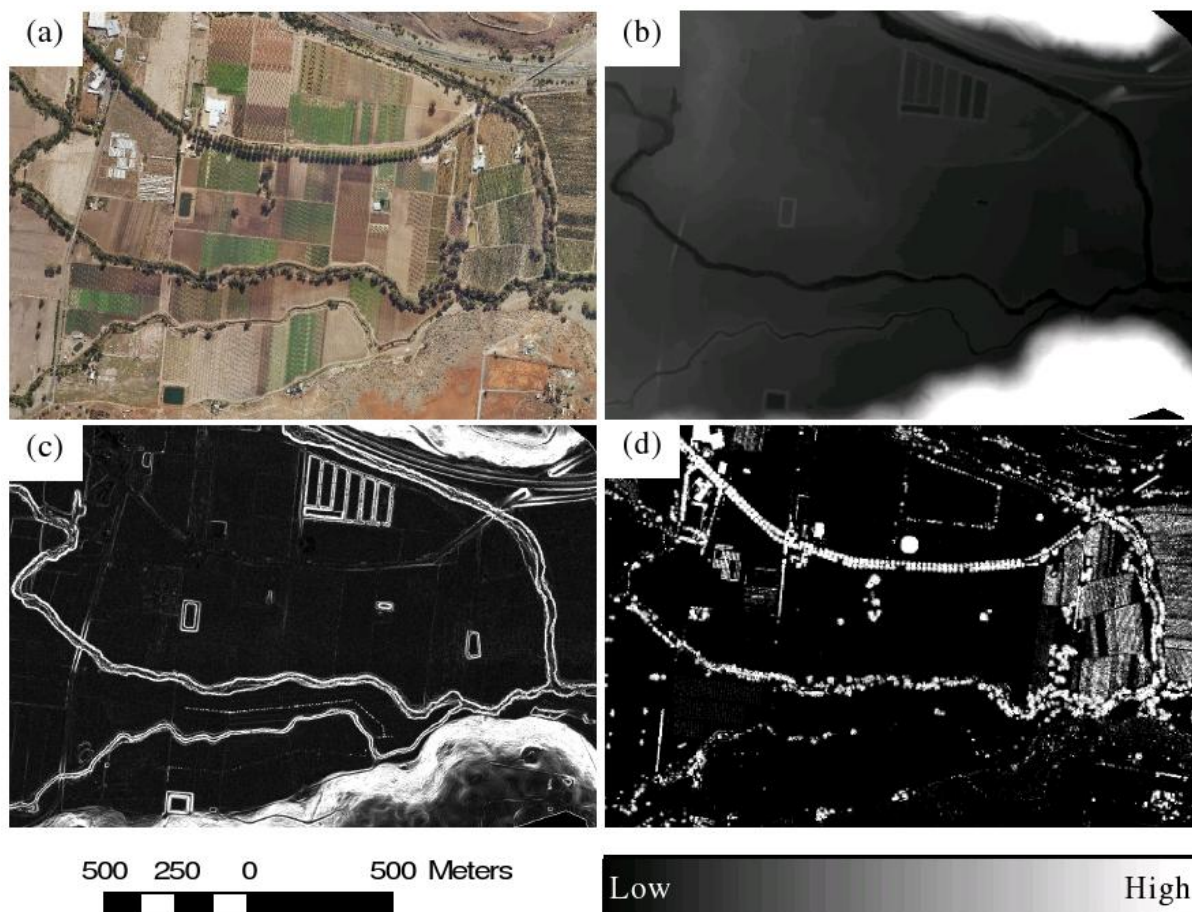
returns were classified as ground or non-ground by the data provider using proprietary software. The flying height when capturing the LiDAR data was approximately 1,500 m above ground level. The maximum scan angle was set to 40 ° with a 25% overlap between different flight lines. The estimated vertical and horizontal accuracies were <0.20 m and <0.75 m respectively. GPS base stations were used for support to improve the geometric accuracy of the dataset. The LiDAR data were deemed suitable for integration with the field data despite the time gap between the data acquisitions. This assumption was based on existing riparian field measurements and photographs from 2004 provided by the Victorian Department of Sustainability and Environment [34]. Fourteen field sites visited in 2004 were revisited during the field campaign in 2008 to compare field measurements of bank and riparian zone widths and associated photographs. This comparison and rainfall data indicating lower than average rainfalls between 2005 and 2008 [35] confirmed that no changes in streambed and riparian zone extents had occurred within the study area between the LiDAR and field data acquisitions.

The following three LiDAR products were produced for use in the GEOBIA: DTM; terrain slope; and fractional cover count converted to PPC (Figure 2). The DTM was produced at a pixel size of 1 m using an inverse distance weighted interpolation of returns classified as ground hits. From this DTM, the rate of change in horizontal and vertical directions was calculated to produce a terrain slope layer measured in degrees [36,37]. Fractional cover count defined as one minus the gap fraction probability, *i.e.*, the probability of an unobstructed path between the point and range in a set direction [38], was calculated from the proportion of counts from first returns >2 m above ground level within 5 m × 5 m pixels. The height threshold of 2 m above ground was also used in the field for measuring PPC. A detailed explanation of calculating PPC from fractional cover counts can be found in Armston *et al.* [39]. These LiDAR derived raster products were used for GEOBIA to map the streambed and riparian zone extents. A shapefile representing the location of the stream centers within the study area was provided by the Victorian Department of Sustainability and Environment and also used in the GEOBIA.

#### 2.4. Classifying Streambeds

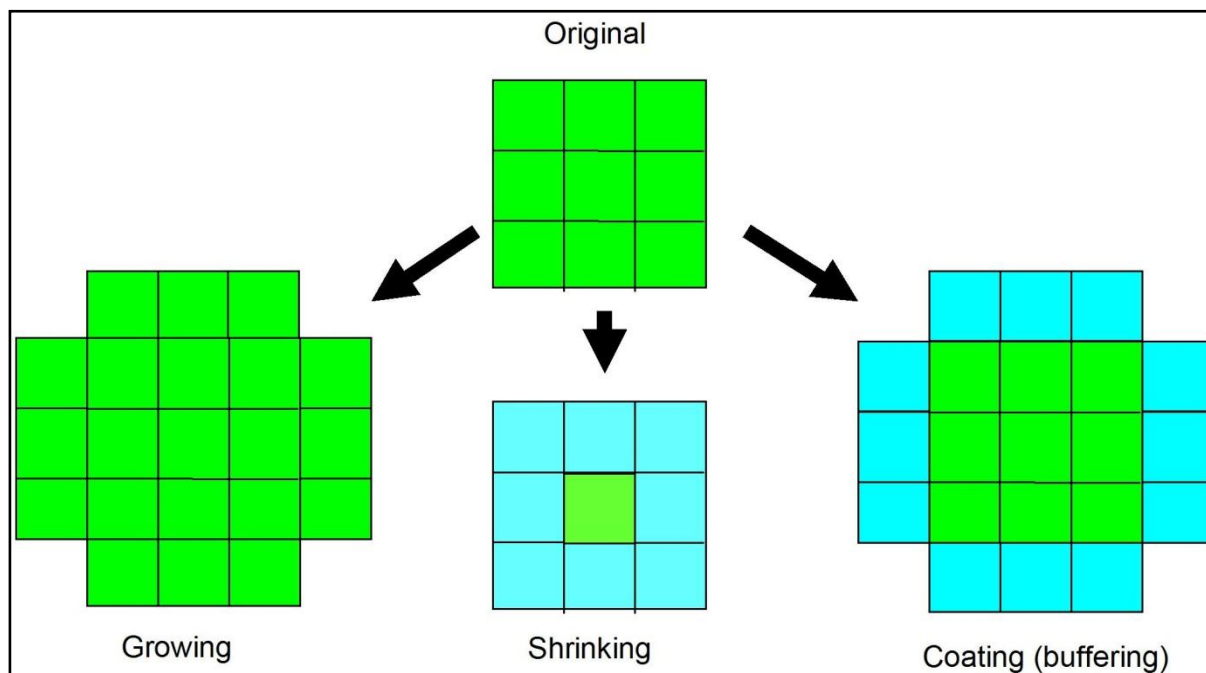
The streambed extent was defined as the continuous flat low-lying area from the toe of one bank to the toe of the opposite bank, which is generally where water is flowing. Mapping the extent of streambeds cannot be done simply by setting an elevation threshold from a DTM, as upstream areas will have different elevations to downstream areas. Johansen *et al.* [8] developed an approach using the DTM and terrain slope layers, but the processing was found very time-consuming and only useful for homogenous riparian zones in a natural state within savanna woodlands. In this case, the study area was much more complex represented urbanized, agricultural and forested areas. Cognition network language (CNL) in the software eCognition 8 was used for the development of a rule set for time-efficient mapping of the streambed extent using the DTM, slope and rasterized polyline representing the approximate stream centerline. CNL offers a multitude of options related to object-based image analysis. It supports programming tasks like branching, looping, and the use of variables. More specifically, it enables addressing single objects and supports manipulating and supervising the process of generating scaled objects in a region-specific manner.

**Figure 2.** Optical UltracamD image (a) showing part of the study area as a true color composite and corresponding LiDAR derived raster products, including: (b) DTM; (c) slope; and (d) PPC. Bright areas indicate high values and dark areas indicate low values.



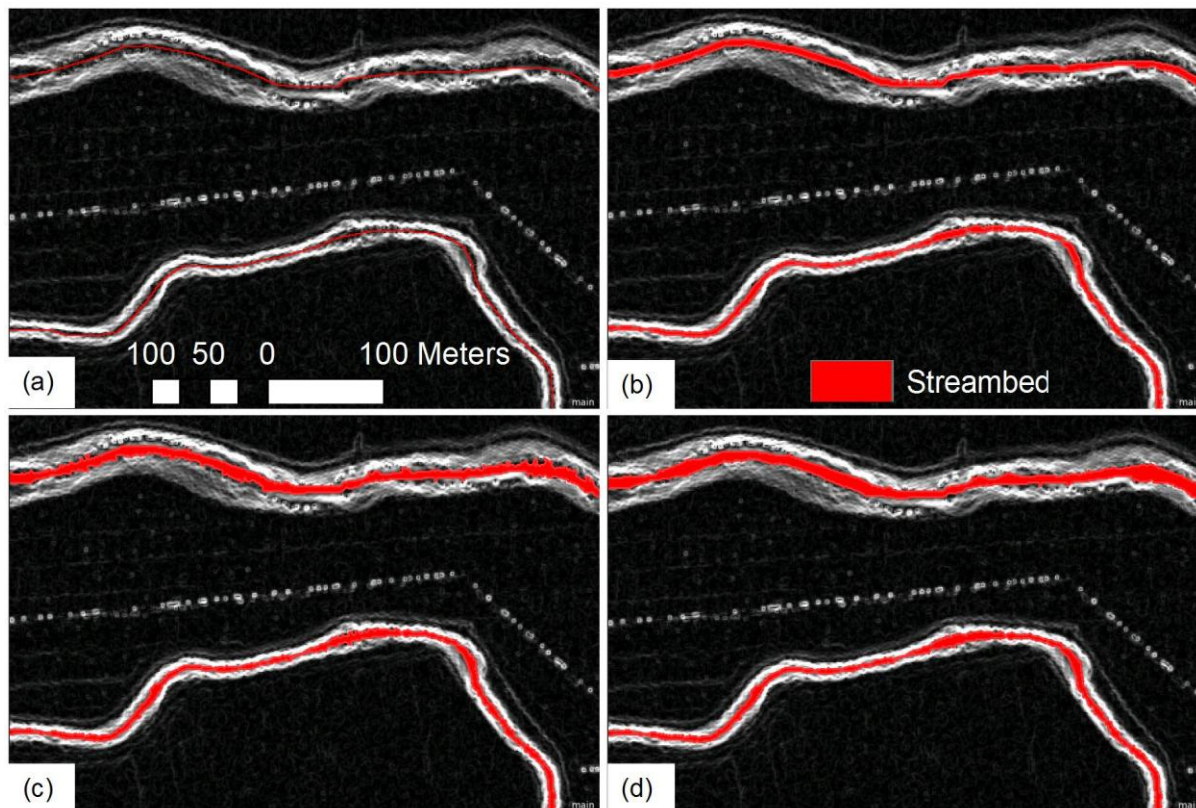
Pixel-based object resizing algorithms are new algorithms introduced in eCognition 8, which allow the growing, shrinking and coating of objects by directly connecting to single pixels of the underlying data sets. The growing mode adds and merges one row of pixels on the outside of an existing object. Through multiple loops, multiple layers of pixels can be added. The shrinking mode subtracts one row of pixels from an original object through classification of this row of objects as a separate class. The coating mode adjoins one row of pixels around an existing object and classifies it to a separate class, similar to buffering (Figure 3) [40]. Conditions can be set for adding, subtracting and adjoining layers of pixels, e.g., only pixels below a set threshold may be considered. Through looping, multiple layers of pixels can be added, subtracted or adjoined. These algorithms may replace some computational intensive object growing algorithms, which rely heavily on topological calculations between objects (polygons).

**Figure 3.** Pixel-based object resizing modes showing the principles of growing (adds one row of pixels on the outside of the existing object), shrinking (subtracts one row of pixels along the outer edge of the object) and coating (adjoins one row of pixels on the outside of the existing object).



Initially, a multi-threshold segmentation was used to classify the rasterized stream centerline with pixel values of 1. As all other pixels within this layer had pixel values of 0 a set threshold of 0.9 was used to classify pixels with a value  $> 0.9$  representing the polyline while pixels  $< 0.9$  remained unclassified (Figure 4(a)). The next stage used the pixel-based object resizing algorithm to grow the stream centerline through two loops as long as the slope did not exceed  $12^\circ$  and the unclassified candidate pixels, *i.e.*, pixels surrounding the stream centerline, were  $< 0.5$  m in elevation compared to the stream centerline. This approach was used to widen the stream centerline to 5 m through the two loops. A width of 5 m was chosen as all streams were wider than 5 m and as the widening of the centerline permitted more pixels to be included in the contextual relations of neighboring pixels in the subsequent steps. Subsequently, the pixel-based object growing was used to grow the widened stream centerline as long as the unclassified candidate pixels surrounding the widened stream centerline were  $< 0.01$  m in elevation compared to the widened stream centerline using an empirically derived surface tension of  $> 0.2$  within an  $11 \times 11$  pixel window (Figure 4(b)). Surface tension looks at the relative area of classified pixels within a moving window centered at the candidate pixel, *i.e.*, edge layer of pixels of an object, to optimize the object shape. The pixel-based object resizing algorithm was then used to further grow the streambed as long as the slope did not exceed  $12^\circ$  and the unclassified candidate pixels were  $< 0.08$  m in elevation compared to the stream centerline. These thresholds were empirically derived. A surface tension of  $> 0.5$  within an  $11 \times 11$  pixel window was used this time to smooth the border of the resizing object (Figure 4(c)). Finally, objects enclosed by the streambed were merged with the streambed objects (Figure 4(d)).

**Figure 4.** Mapping the streambed from the LiDAR derived DTM and slope layers and a rasterized polyline representing the stream centerline. The slope layer is used as a backdrop. **(a)** Classification of stream centerline using multi-threshold segmentation; **(b)** Pixel-based object growing of centerline; **(c)** Further pixel-based object growing based on the DTM and slope; **(d)** Final extent of streambed after merging.



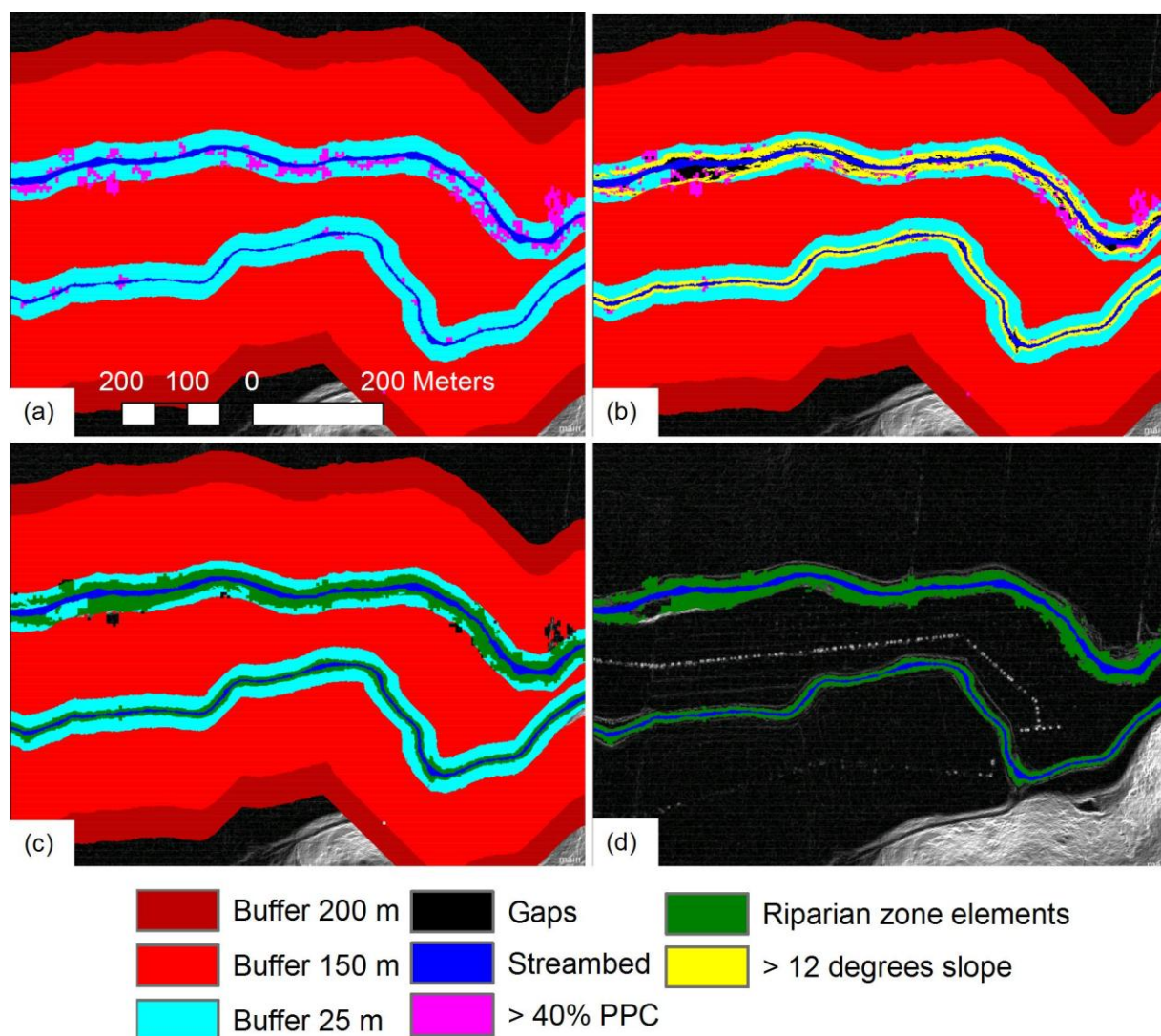
### 2.5. Classifying Riparian Zones

The rule set used for classification of the streambeds and riparian zones was based on the approach developed by Johansen *et al.* [8]. However, as this approach used several computation-intensive segmentation (e.g., pixel-sized chessboard segmentations) and regionalization steps based on topological relations (e.g., image object fusion, merging and region-growing algorithms), it was found very time-consuming for use over large areas. The approach presented here focused on more time-effective mapping of the riparian zones using new algorithms implemented in eCognition 8.

Riparian zone extent was defined as the area between the streambed and the external perimeter defined by a significant change in terrain slope (top of bank) and vegetation structure and species. This definition corresponds to the one used by the Department of Sustainability and Environment [41] and was found useful because of the highly modified landscape of the study area, with well-defined lowland channels and vegetation structure and species often changing abruptly due to bordering cultivation, grazing and urban development. The classification of the streambed was used to identify the streamside edge of the riparian zone. A number of steps were used for mapping the riparian zones, again focusing on the use of the pixel-based object resizing algorithm. To include distance measures around the streambed, it was not sufficient only to use the pixel-based growing algorithms starting

from the streambed, as non-connected elements were missing. Therefore, three different buffers in relation to the streambed were created (25 m, 150 m, and 200 m from the stream) to correspond to distance measures required within the individual processes of the rule set. The distance buffers were first created using the coating mode and then followed by the pixel-based object resizing algorithm using the shrinking mode. The shrinking algorithm was initially used to map PPC > 40% (Figure 5(a)). The shrinking algorithm was then used within the 25 m buffer to identify areas with >12° terrain slope, as these can be assumed to belong to the stream bank and hence riparian zone even if not vegetated. These thresholds were based on field observations.

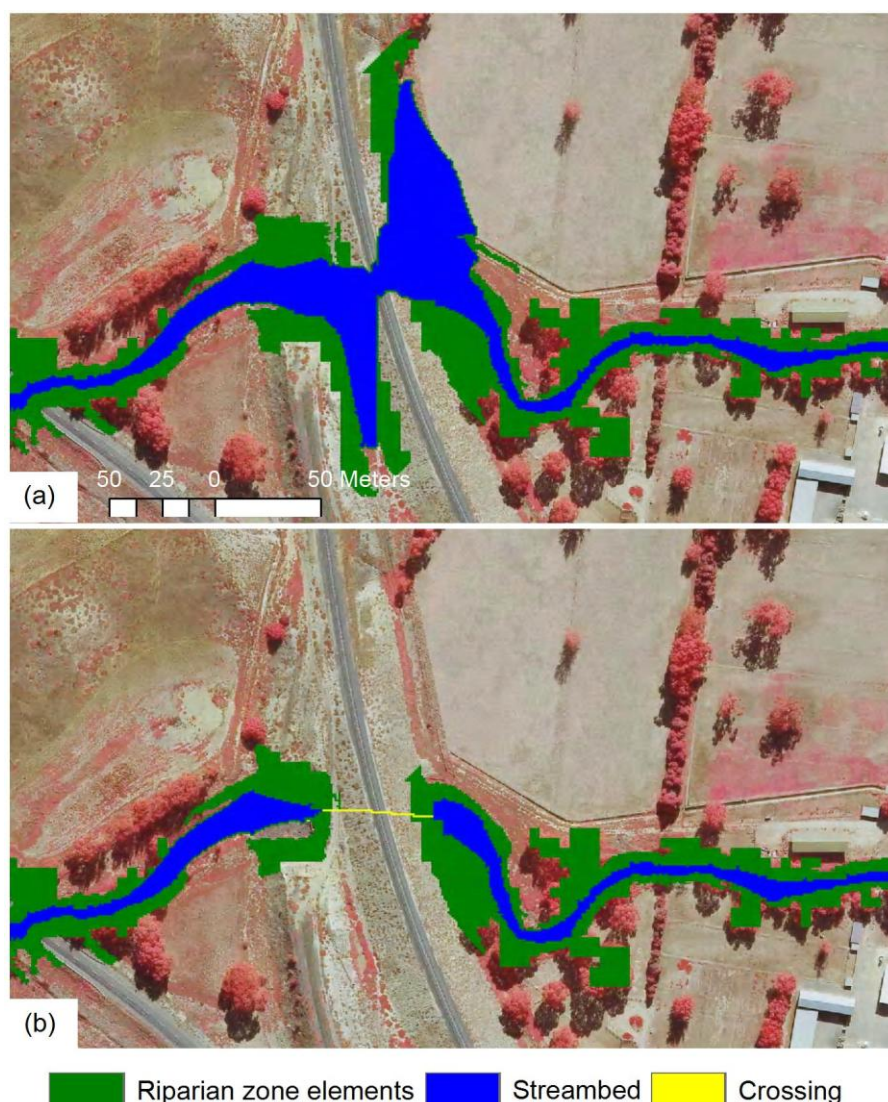
**Figure 5.** Mapping riparian zone extent from the LiDAR derived DTM, slope, PPC and streambed layers. The slope layer is used as a backdrop. (a) Buffers and mapping of streamside woody vegetation with more than 40% plant projective cover; (b) Mapping of stream banks based on slope; (c) Mapping of riparian zone extent adjusted based on elevation in relation to the streambed; (d) Adjusting riparian zone edges based on PPC.



Gaps enclosed by the streambed and with PPC > 40% and bank slope > 12° were also assumed to be part of the riparian zone (Figure 5(b)). Those riparian elements, including objects with >40% PPC,

>12° bank slope and gaps were merged and those objects not in contact with the streambed were omitted. Elevation differences between the streambed and the external perimeter of the riparian zone provided very useful information for mapping riparian zone extent to ensure riparian zones do not extend into non-riparian areas in hilly landscapes. Based on field observations, a DTM value of 5 m above the streambed was set as the maximum elevation for riparian zones within a distance of 150 m from the streambed using relational topological features between objects and classes (Figure 5(c)). Riparian canopy vegetation extending beyond the edge of the bank top till provides riparian zone functions in terms of habitat and corridor continuity. Therefore, riparian canopy along the external perimeter was included as part of the riparian zone when PCC was > 60%. This threshold was based on field measurements of PPC within the riparian zones. The shrinking algorithm was used for this process (Figure 5(d)).

**Figure 6.** Example of streambed and riparian zone classification for an area with a railway crossing the stream. (a) Classification issues of the stream and riparian zone because of distinct elevation and slope changes caused by the railway crossing; (b) Improved classification where the railway crossing has been classified based on distinct elevation differences.



Through the implementation of the rule set, streambed and riparian zone classification issues were recognized in areas with wide stream crossings such as some bridges and railway crossings (Figure 6(a)). A characteristic of all crossings within the study area was an elevation increase along the stream centerline, e.g., where bridges were constructed across the streams. These local but significant changes in the elevation of the streambed were isolated by applying a chessboard segmentation with an object size of 1 to convert the stream centerline into individual pixels after the initial multi-threshold segmentation to classify the streambed (Figure 4(a)). A spectral difference segmentation of the stream centerline with a maximum elevation difference of 2 m using the DTM layer was applied to merge sections of the stream centerline with similar elevation. Neighboring image objects, *i.e.*, pixels because of the chessboard segmentation applied, were merged if the difference between their mean elevation was below 2 m. Hence, sections of the stream centerline exhibiting distinct elevation change, e.g., where bridges were crossing the streams, ended up with short segments compared to natural stream sections with limited spatial elevation differences within the study area. To separate streambed and riparian zone areas with and without crossings, segments with a border length of less than 80 pixels (80 m) were classified as crossings and subsequently merged. These crossings were not taken into account for the following streambed and riparian zone classification (Figure 6(b)).

## 2.6. Validation

The field measurements of streambed and riparian zone widths were used for validation of the GEOBIA classification results. The validation was performed using scatter plots and calculating the related coefficient of determination ( $R^2$ ) and root mean square error (RMSE). A total of 35 field measurements of streambed and riparian zone widths were used for the validation of the classification.

## 3. Results and Discussion

Substitution of most of the time and power consuming segmentation and object growing processes with the pixel-based object resizing algorithm using the growing, shrinking and coating modes proved very effective for reducing the processing time. A significant reduction in processing time, now approximately 25 times faster was possible without affecting the mapping accuracies. Also, tiling of the study area was not necessary anymore compared to the approach of Johansen *et al.* [8], which required multiple tiles to be developed and processed individually because of the use of chessboard segmentations producing very large numbers of objects. Reducing the number of tiles or eliminating the need for tiling and stitching processing avoids errors in the classification due to biases along the tiling edges and intensive post-processing [42]. The new approach developed was also found suitable for application in urbanized, agricultural and forested areas. The mapping results for these environments are presented in Figure 7.

The comparison of field assessed streambed and riparian zone widths with those derived from the LiDAR data and GEOBIA showed high correlation with no distinct outliers (Figure 8). Measurements of streambed width were very accurately mapped, which may have been facilitated by the lack of water in most streams at the time of LiDAR data captured. The measurements of wider streambeds were mainly located within a reservoir, where the toes of the banks were poorly defined because of the very limited bank slopes. This added some uncertainty to the GEOBIA identification of the streambed

edges. LiDAR data with higher point densities may be more suitable for streams with no distinct bank toes to facilitate identification of detailed physical form characteristics of the stream/riparian zone interface to improve mapping accuracies [37].

**Figure 7.** Mapping results showing streambed and riparian zone extent with UltracamD image data used as a backdrop for an (a) agricultural; (b) forested; and (c) urbanized area depicted both without and with the classification result.

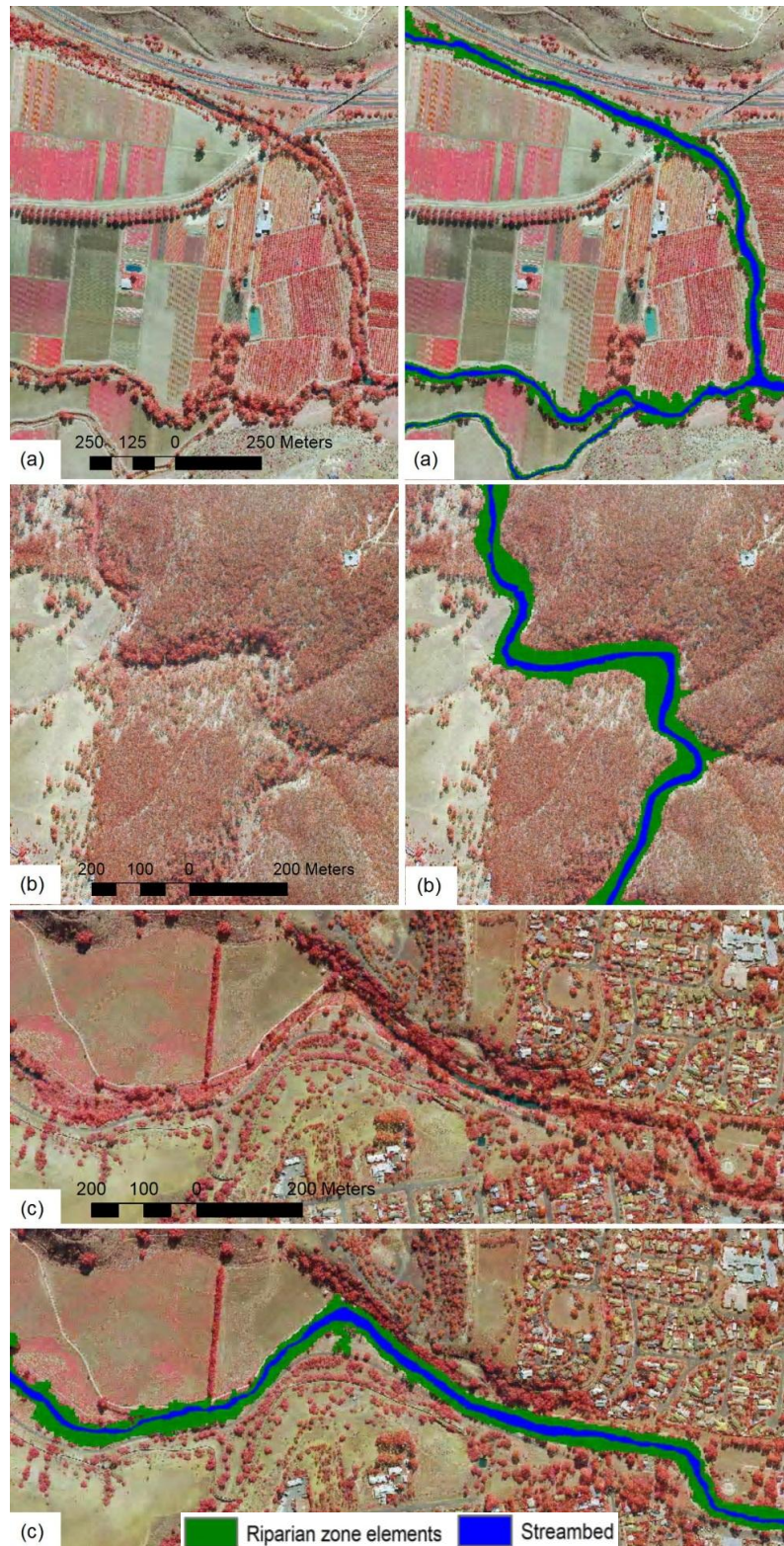
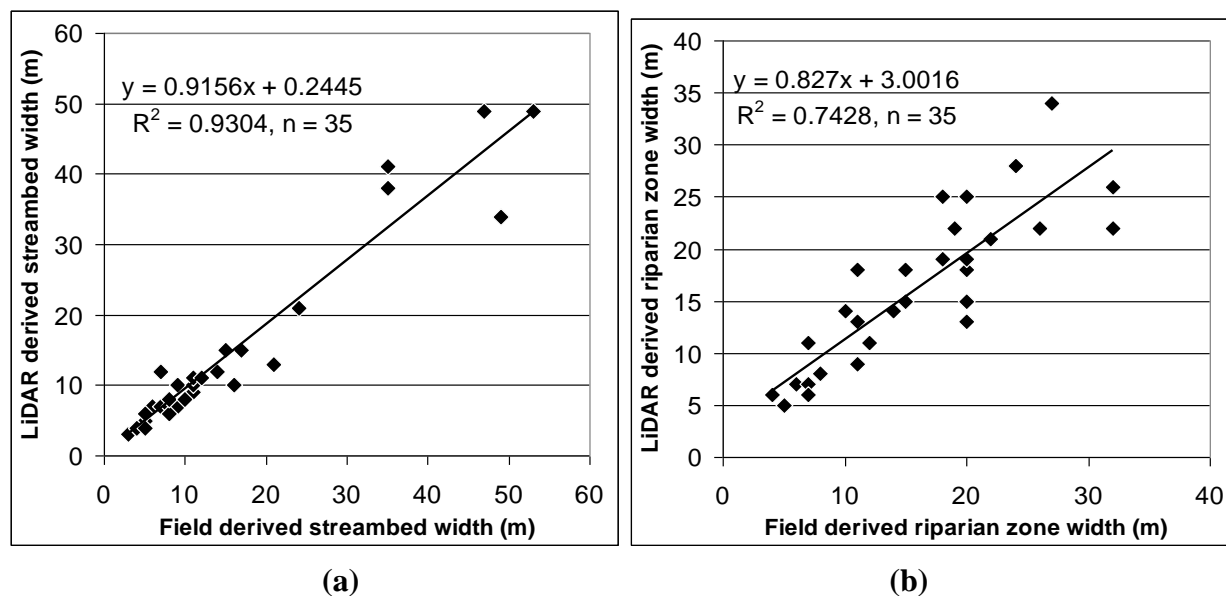


**Figure 8.** Scatter plots and trend lines comparing field and LiDAR derived (a) streambed width and (b) riparian zone width for 35 field sites. (a) RMSE = 3.6 m,  $P < 0.001$ ; (b) RMSE = 3.9 m,  $P < 0.001$ .



Field and LiDAR derived measurements of riparian zone width matched up in most cases, but did generally show larger variation than the streambed width measurements. In the majority of cases, where riparian zone width was underestimated, the riparian zone had limited canopy cover appearing on relatively flat stream banks, such as the inside sections of meander bends (Figure 9). Because of the reliance on identification of bank slopes and/or canopy cover bordering the mapped streambeds, the rule set resulted in an underestimation of riparian zone width in some areas. This may be improved in future work through identification of meander bends based on the shape of the streambed and application of specific rule set processes for these areas to facilitate identification of riparian zone extent. This may be done using the DTM to identify the bank top/riparian zone external edge on the outside of meander bends and match this elevation level to the inside of the meander bend to delineate the external riparian zone edge in meander bends with limited bank slope and canopy cover [41].

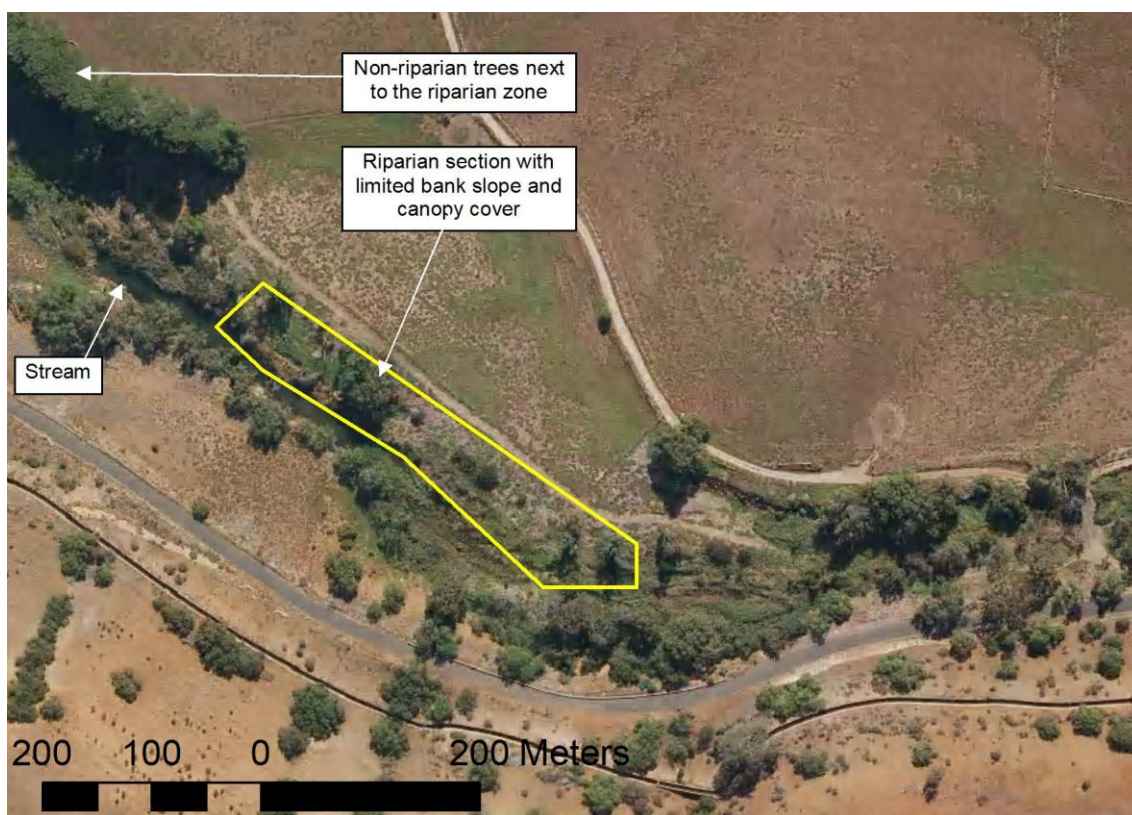
In some situations, the riparian zone width was overestimated if dense non-riparian canopy occurred next to the riparian zone (Figure 9). The rule set may be improved to prevent non-riparian canopy cover from being mapped as part of the riparian zone, if these trees occur at a terrain elevation above the one identified as the bank top. If bank top identification on the one side of the stream with dense non-riparian canopies bordering the riparian zone is not possible, the elevation of the bank top on the opposite side of the stream may be used to determine whether or not to include tree canopies as part of the riparian zone. However, this will require complex rule set development to match two opposite stream bank sides, because of the non-linear shape of streams and riparian zone edges.

#### 4. Conclusions

This research presented a GEOBIA approach for accurate and time-effective mapping of streambed and riparian zone extents in a complex rural urban environment based on LiDAR derived DTM, terrain slope and PPC layers as well as an additional rasterized stream centerline shapefile. To improve

processing power and time, the rule set relied heavily on the new pixel-based object resizing algorithms in eCognition 8. Through a combination of growing, shrinking and coating functions, the streambed and riparian zone widths were mapped with  $R^2$  values of 0.93 and 0.74, respectively in relation to field measurements. The developed rule sets also enabled processing of larger areas than previous research without using tiling and stitching functions. As the study area presented a number of different riparian environments from urban and agricultural sites to natural and hilly areas, the rule set may be applicable to other areas for streambed and riparian extent mapping. This is facilitated by the definition of variables at the beginning of the rule set, allowing a simple and fast calibration for other areas/conditions if needed. However, further research is required to reduce the under- and over-estimation of riparian zone width in areas with limited canopy cover and bank slope as well as areas with dense non-riparian canopies bordering the riparian zones.

**Figure 9.** Example of riparian zone section (outlined in yellow) with very limited bank slope and canopy cover, which caused underestimation of riparian zone width in some areas. Non-riparian trees next to the riparian zone caused overestimation of riparian zone width. UltracamD image data used for illustration.



## Acknowledgements

Michael Hewson and Eric Ashcroft from the Centre for Spatial Environmental Research at the University of Queensland, Australia, and John Armston from the Remote Sensing Centre at QLD Department of Environment and Resource Management, Australia and Paul Wilson, Sam Marwood and John White from the Department of Sustainability and Environment, Victoria provided significant help with fieldwork and image processing.

## References

1. Naiman, R.J.; Decamps, H. The ecology of interfaces: Riparian zones. *Ann. Rev. Ecol. Syst.* **1997**, *28*, 621-658.
2. Apan, A.A.; Raine, S.R.; Paterson, M.S. Mapping and analysis of changes in the riparian landscape structure of the Lockyer Valley catchment, Queensland, Australia. *Landscape Urban Plan.* **2002**, *59*, 43-57.
3. Werren G.; Arthington, A. The assessment of riparian vegetation as an indicator of stream condition, with particular emphasis on the rapid assessment of flow-related impacts. In *Landscape Health of Queensland*; Shapcott, A., Playford, J., Franks, A.J., Eds.; The Royal Society of Queensland: St Lucia, QLD, Australia, 2002; pp. 194-222.
4. Johansen, K.; Phinn, S.; Lowry, J.; Douglas, M. Quantifying indicators of riparian condition in Australian tropical savannas: Integrating high spatial resolution imagery and field survey data. *Int. J. Remote Sens.* **2008**, *29*, 7003-7028.
5. Johansen, K.; Phinn, S.; Dixon, I.; Douglas, M.; Lowry, J. Comparison of image and rapid field assessments of riparian zone condition in Australian tropical savannas. *For. Ecol. Manage.* **2007**, *240*, 42-60.
6. Hurtt, G.; Xiao, X.; Keller, M.; Palace, M.; Asner, G.P.; Braswell, R.; Brondizio, E.S.; Cardoso, M.; Carvalho, C.J.R.; Fearon, M.G.; *et al.* IKONOS imagery for the Large Scale Biosphere-Atmosphere Experiment in Amazonia (LBA). *Remote Sens. Environ.* **2003**, *88*, 111-127.
7. Johansen, K.; Roelfsema, C.; Phinn, S. Special feature-high spatial resolution remote sensing for environmental monitoring and management. *J. Spatial Sci.* **2008**, *52*, 43-47.
8. Johansen, K.; Arroyo, L.A.; Armston, J.; Phinn, S.; Witte, C. Mapping riparian condition indicators in a sub-tropical savanna environment from discrete return LiDAR data using object-based image analysis. *Ecol. Indic.* **2010**, *10*, 796-807.
9. Johansen, K.; Phinn, S.; Witte, C. Mapping of riparian zone attributes using discrete return LiDAR, QuickBird and SPOT-5 imagery: Assessing accuracy and costs. *Remote Sens. Environ.* **2010**, *114*, 2679-2691.
10. Blaschke, T.; Strobl, J. What's wrong with pixels? Some recent developments interfacing remote sensing and GIS. *GIS-Zeitschrift für Geoinformationssysteme* **2001**, *14*, 12-17.
11. Burnett, C.; Blaschke, T. A multi-scale segmentation/object relationship modelling methodology for landscape analysis. *Ecol. Model.* **2003**, *168*, 233-249.
12. Blaschke, T.; Burnett, C.; Pekkarinen, A. New contextual approaches using image segmentation for object-based classification. In *Remote Sensing Image Analysis: Including the Spatial Domain*; De Meer, F., de Jong, S., Eds.; Kluwer Academic Publishers: Dordrecht, the Netherlands, 2004; pp. 211-236.
13. Blaschke, T. Object based image analysis for remote sensing. *ISPRS J. Photogramm. Remote Sens.* **2010**, *65*, 2-16.
14. Benz, U.C.; Hofmann, P.; Willhauck, G.; Lingenfelder, I.; Heynen, M. Multi-resolution, object-oriented fuzzy analysis of remote sensing data for GIS-ready information. *ISPRS J. Photogramm. Remote Sens.* **2004**, *58*, 239-258.

15. Liu, Y.; Li, M.; Mao, L.; Xu, F. Review of remotely sensed imagery classification patterns based on object oriented image analysis. *Chinese Geogr. Sci.* **2006**, *16*, 282-288.
16. Lang, S. Object-based image analysis for remote sensing applications: Modeling reality—dealing with complexity. In *Object Based Image Analysis*; Blaschke, T., Lang, S., Hay, G.J., Eds.; Springer: Heidelberg/Berlin, Germany, 2008; pp. 1-25.
17. Blaschke, T.; Lang, S.; Hay, G.J. *Object Based Image Analysis*; Springer: Berlin, Germany, 2008; p. 817.
18. Haralick, R.M.; Shapiro, L. Survey: Image segmentation techniques. *Comput. Vis. Graph. Image Process.* **1985**, *29*, 100-132.
19. Pal, R.; Pal, K. A review on image segmentation techniques. *Pattern Recogn.* **1993**, *26*, 1277-1294.
20. Hay, G.J.; Blaschke, T.; Marceau, D.J.; Bouchard, A. A comparison of three image-object methods for the multiscale analysis of landscape structure. *ISPRS J. Photogramm. Remote Sens.* **2003**, *57*, 327-345.
21. Zhan, Q.F.; Molenaar, M.; Tempfli, K.; Shi, W. Quality assessment for geo-spatial objects derived from remotely sensed data. *Int. J. Remote Sens.* **2005**, *26*, 2953-2974.
22. Hay, G.J.; Castilla, G. Geographic Object-Based Image Analysis (GEOBIA): A new name for a new discipline. In *Object Based Image Analysis*; Blaschke, T., Lang, S., Hay, G., Eds.; Springer: Berlin, Germany, 2008; pp. 93-112.
23. Kettig, R.; Landgrebe, D. Classification of multispectral image data by extraction and classification of homogeneous objects. *IEEE Trans. Geosci. Electron.* **1976**, *GE-14*, 19-26.
24. Neubert, M.; Herold, H.; Meinel, G. Assessing image segmentation quality—concepts, methods and application. In *Object Based Image Analysis*; Blaschke, T., Lang, S., Hay, G.J., Eds.; Springer: Berlin, Germany, 2008; pp. 760-784.
25. Ke, Y.; Quackenbush, L.J.; Im, J. Synergistic use of QuickBird multispectral imagery and LIDAR data for object-based forest species classification. *Remote Sens. Environ.* **2010**, *114*, 1141-1154.
26. Hay, G.J.; Marceau, D.J.; Dube, P.; Bouchard, A. A multiscale framework for landscape analysis: Object-specific analysis and upscaling. *Landscape Ecol.* **2001**, *16*, 471-490.
27. Langanke, T.; Burnett, C.; Lang, S. Assessing the mire conservation status of a raised bog site in Salzburg using object-based monitoring and structural analysis. *Landscape Urban Plan.* **2007**, *79*, 160-169.
28. Laliberte, A.S.; Fredrickson, E.L.; Rango, A. Combining decision trees with hierarchical object-oriented image analysis for mapping arid rangelands. *Photogramm. Eng. Remote Sensing* **2007**, *73*, 197-207.
29. Stow, D.; Hamada, Y.; Coulter, L.; Anguelova, Z. Monitoring shrubland habitat changes through object-based change identification with airborne multispectral imagery. *Remote Sens. Environ.* **2008**, *112*, 1051-1061.
30. Tiede, D.; Lang, S.; Hoffmann, C. Domain-specific class modelling for one-level representation of single trees. In *Object-Based Image Analysis*; Blaschke, T., Lang, S., Hay, G., Eds.; Springer: Berlin, Germany, 2008; pp. 133-151.

31. Gibbes, C.; Adhikari, S.; Rostant, L.; Southworth, J.; Qiu, Y. Application of object based classification and high resolution satellite imagery for savanna ecosystem analysis. *Remote Sens.* **2010**, *2*, 2748-2772.
32. Stow, D. Geographic object-based image change analysis. In *Handbook of Applied Spatial Statistics*; Fischer, M.M., Getis, A., Eds.; Springer: Berlin, Germany, 2010; Volume 4, pp. 565-582.
33. Earth Tech. *Geomorphic Overview of Waterways in the Werribee River Catchment*; Melbourne Water: Melbourne, VIC, Australia, 2006.
34. Department of Sustainability and Environment. *Index of Stream Condition: The Second Benchmark of Victorian River Condition*; Department of Sustainability and Environment, The State of Victoria: Melbourne, VIC, Australia, 2005.
35. BoM. *Climate Data Online*; Bureau of Meteorology, Australian Government: Melbourne, VIC, Australia, 2008. Available online: <http://www.bom.gov.au/climate/data/> (accessed on 5 May 2011).
36. Anderson, E.S.; Thompson, J.A.; Austin, R.E. LIDAR density and linear interpolation effects on elevation estimates. *Int. J. Remote Sens.* **2005**, *26*, 3889-3900.
37. Hodgson, M.E.; Bresnahan, P. Accuracy of airborne lidar-derived elevation: Empirical assessment and error budget. *Photogramm. Eng. Remote Sensing* **2004**, *70*, 331-339.
38. Lovell, J.L.; Jupp, D.L.B.; Culvenor, D.S.; Coops, N.C. Using airborne and ground-based ranging lidar to measure canopy structure in Australian forests. *Can. J. Remote Sens.* **2003**, *29*, 607-622.
39. Armston, J.; Denham, R.; Danaher, T.; Scarth, P.; Moffiet, T. Prediction and validation of foliage projective cover from Landsat-5 TM and Landsat-7 ETM+ imagery for Queensland, Australia. *J. Appl. Remote Sens.* **2009**, *3*, 1-28.
40. eCognition. *eCognition Developer 8.0.1 User Guide*; Document Version 1.2.1; Definiens AG: Munich, Germany, 2010.
41. Department of Sustainability and Environment. *Index of Stream Conditions Users Manual*, 3rd ed.; Department of Sustainability and Environment, The State of Victoria: Melbourne, VIC, Australia, 2006.
42. Tiede, D.; Hoffmann, C. Process Oriented Object-Based Algorithms for Single Tree Detection Using Laser Scanning Data. In *Proceedings of the EARSeL-Workshop on 3D Remote Sensing in Forestry*, Vienna, Austria, 14–15 February 2006; pp. 151-156.